2018

Pressure Drop Model For Condensation From Superheated Vapor

Jiange Xiao
ACRC, the University of Illinois, jxiao10@illinois.edu

Predrag S. Hrnjak
pega@illinois.edu

Pressure Drop Model For Condensation From Superheated Vapor

Jiange XIAO[1], Pega HRNJAK[1,2]*

[1]University of Illinois at Urbana-Champaign, Department of Science and Engineering,

Urbana, IL, USA

Jxiao10@illinois.edu, pega@illinois.edu

[2]Creative Thermal Solutions,

Urbana, IL, USA

* Corresponding Author

ABSTRACT

A new pressure drop model based on flow regime map is proposed for condensation inside horizontal smooth round tubes accounting for the non-equilibrium in a vapor compression system. Conventionally, a pressure drop model for two-phase flow only accounts for the prediction between bulk quality 1 and 0. The temperature gradient during condensation, however, creates the non-equilibrium that guarantees two-phase flow beyond bulk quality 1 and 0. The new model determines the onset and end of condensation by tracing the development of the liquid film when the superheated vapor is condensed on the tube wall. The flow regime map designed specifically for condensation from superheated vapor is used to predict the flow regime when the flow is two-phase. Two flow regime transitions are recognized. One is from annular flow to the stratified flow under low mass fluxes; the other is from annular flow to the intermittent flow under high mass fluxes. The annular flow is treated as a uniform ring; the stratified flow is treated as a combination of annular flow on the upper part of the tube and liquid pool at the bottom part of the tube; the intermittent flow is treated as a combination of annular flow and single-phase liquid flow that occurs intermittently. The weights designated to each flow regime is calculated from the void fraction model that also accounts for non-equilibrium and is used in the flow regime map. The prediction of the new model is compared with experimental data of R32, R134a and R1233zd(E) mass fluxes from 100 to 400 kg/m^2-s, heat fluxes from 5 to 15 kW/m^2 and tube diameters of 4.0 and 6.1 mm at saturation temperatures of 30 ^{o}C. The comparison shows that the new model provides good agreements with experimental data. Additionally, by accounting for the non-equilibrium in the condensation process, the new model seamlessly connects the single-phase and two-phase regions with the corresponding mechanisms that occurs in a real vapor compression system.

1. INTRODUCTION

Condensation is usually considered as a heat rejection process when the mass ratio of vapor and the whole fluid changes from 1 to 0. The pressure drop during a condensation process typically includes three parts: frictional, acceleration and gravitational pressure drop. Frictional pressure drop is the most discussed component in literature. Gravitational pressure drop will not be discussed in this paper. In condensation, deceleration pressure gain is usually mentioned as the sole effect of having the heat transfer. In reality, the impacts on pressure drop due to having heat exchanged out of the refrigerant are a lot more than just having fluid velocity reduced. It has been shown by Xiao and Hrnjak (2018) that the pressure drop where there is temperature gradient inside has shifted the mechanism towards two-phase even when the specific enthalpy indicates the refrigerant to be single-phase. The discrepancy between the pressure drop mechanism in reality and thermodynamic point of view creates a deviation between experimental data and model predictions that cannot be resolved unless the non-equilibrium effects are taken into account.

Kondo and Hrnjak (2011a, 2011b, 2012) and Agarwal and Hrnjak (2013) had extensive measurements on the HTC in the region where the two-phase mechanism comes into play because the tube inner wall temperature drops below saturation temperature. Even though the specific enthalpy suggests superheated vapor inside the tube, the tube wall is covered by liquid film and latent heat raises the HTC to be several times of what is predicted by the single-phase HTC correlations such as Gnielinski (1976) and Dittus-Boelter (1930). Two more regions named as condensing superheated (CSH) and condensing subcooled regions (CSC) are brought up. Meyer and Hrnjak (2017) then proved the existence of liquid film in the tube through the flow visualization and film thickness measurement of R134a. By tracing the development of the film and calculating the real onset and end of the condensation, Xiao and Hrnjak (2016, 2017a, 2017b) purposed the new void fraction, flow regime map and HTC model for condensation from superheated vapor accounting for the non-equilibrium effects. The deviation in pressure drop between the experimental data and predictions mentioned by Xiao and Hrnjak (2018) is not addressed in the literature.

2. THE NEW PRESSURE DROP MODEL

2.1 Finding the beginning and the end

$$T_{b,onset} = T_{sat} + \frac{Q}{HTC_{onset}} \tag{1}$$

$$T_{b,end} = T_{sat} - 0.33\frac{Q}{HTC_{end}} \tag{2}$$

$$x_{sup} = \frac{h - h_{end}}{h_{onset} - h_{end}} \tag{3}$$

Eq. (1-3) are used to calculate the real onset and end of the condensation as well as the superficial quality. Eq. (1) finds the beginning of the CSH region. The criteria for the first droplet to form is the tube wall temperature being saturation temperature. The HTC at the onset of the condensation is calculated from the single-phase heat transfer correlations such as Dittus-Boelter (1930) or Gnielinski (1976). Since the bulk temperature of the flow is needed for the HTC calculation, iteration is needed to solve Eq. (1). The criteria for the last vapor to disappear is the highest temperature in the tube being equal to the saturation temperature. Because the temperature profile inside the tube at the end of the condenser is unlikely to be linear, an empirical constant 0.33 is needed to represent the effect of it. Iteration is also required for Eq. (2). The superficial quality is first defined by Xiao and Hrnjak (2017a) to show the real onset and end of condensation, which is different from bulk quality in that it abandoned the thermodynamic assumption for the flow.

2.2 Void fraction correlation and flow regime map

$$\varepsilon_h = \left[1 + \left(\frac{1 - x_{sup}}{x_{sup}}\right)\left(\frac{\rho_v}{\rho_l}\right)\right]^{-1} \tag{4}$$

$$\varepsilon_{RA} = \frac{x_{sup}}{\rho_v}\left[1 + 0.12\left(1 - x_{sup}\right)\left(\frac{x_{sup}}{\rho_v} + \frac{1 - x_{sup}}{\rho_l}\right) + \frac{1.18\left(1 - x_{sup}\right)[g\sigma(\rho_L - \rho_V)]^{0.25}}{G\rho_l^{0.5}}\right]^{-1} \quad (5)$$

$$\varepsilon = \frac{\varepsilon_h - \varepsilon_{ra}}{\ln(\frac{\varepsilon_h}{\varepsilon_{ra}})} \quad (6)$$

The void fraction from Xiao and Hrnjak (2017a) is used in this paper and can be calculated from Eq. (4-6). The correlation is modified from the one by El. Hajal et al. (2003). It is basically a compromise between void fraction correlation by Rouhani-Axelson (1970) that takes mass flux into account and the homogenous model. By incorporating superficial quality into the correlation, the predictions from the correlation are extended from the thermodynamic view of condensation to the real onset and end of the process.

The same goes for the flow regime map. Xiao and Hrnjak (2017a) not only extends the application range of the original map by El. Hajal et al. (2003), but also ensures annular flow at the entrance of the condensation, which is validated by the visualization and explained in the paper. The following steps should be taken to draw the flow regime map.

1. Calculate the real onset and end of condensation using Eq. (1-3).
2. Calculate the void fraction using Eq. (4-6).
3. Calculate the stratification angle, dimensionless cross sectional area of liquid and vapor, height of the liquid pool and the perimeter of the liquid-vapor interface using Eq. (7-11).
4. Find the ratio of Weber number and Froude number by Eq. (12)
5. Find $G_{wavy,1}$ by Eq. (13) and determine the minimum value and its corresponding superficial quality, denoted as $G_{wavy,min}$ and $x_{sup,min}$ respectively. Set the values of all the points of $G_{wavy,1}$ after the minimum point to $G_{wavy,min}$.
6. Determine $G_{wavy,2}$ by Eq. (14).
7. Find the transition curve from the annular flow to the stratified wavy flow G_{wavy} by asymptotically adding up $G_{wavy,1}$ and $G_{wavy,2}$ through Eq. (15).
8. Find the transition curve from the stratified wavy flow to the fully stratified flow G_{strat} through Eq. (16).
9. Find the transition line from the annular flow to the intermittent flow x_{IA} through Eq. (17)
10. The flow map is completed.

$$\theta_{strat} = 2\pi - 2\left\{\pi(1-\varepsilon) + \left(\frac{3}{2}\pi\right)^{\frac{1}{3}}\left[1 - 2(1-\varepsilon)^{\frac{1}{3}} - \varepsilon^{\frac{1}{3}}\right] - \frac{\varepsilon}{200}(1-\varepsilon)[1-2(1-\varepsilon)][1+4(1-\varepsilon)^2+4\varepsilon^2]\right\} \quad (7)$$

$$A_l^* = \frac{\pi}{4}(1-\varepsilon) \quad (8)$$

$$A_v^* = \frac{\pi\varepsilon}{4} \quad (9)$$

$$h_l^* = 0.5\left[1 - \cos(\pi - \frac{\theta_{strat}}{2})\right] \quad (10)$$

$$P_l^* = \sin(\pi - \frac{\theta_{strat}}{2}) \quad (11)$$

$$\left(\frac{We}{Fr}\right)_L = \frac{gd^2\rho_l}{\sigma} \quad (12)$$

$$G_{wavy,1} = \left\{\frac{16{A_v^*}^3 gd\rho_v\rho_l}{x_{sup}^2\pi^2[1-(2h_l^*-1)^2]^{0.5}}\left[\frac{\pi^2}{25{h_l^*}^2}\left(\frac{We}{Fr}\right)_l^{-1.023} + 1\right]\right\}^{0.5} + 100 - 50\mathrm{e}^{-\frac{(\mathrm{x}^2-0.97)^2}{x(1-x)}} \quad (13)$$

$$G_{wavy,2} = G_{wavy,min}\left(1 - \frac{x_{sup} - x_{sup,min}}{1 - x_{sup,min}}\right)^{0.5} \quad (14)$$

$$G_{wavy} = G_{wavy,1}(1-x) + G_{wavy,2}x \quad (15)$$

$$G_{strat} = \left[\frac{226.3^2 A_v^{*2} A_l^* \rho_v (\rho_l - \rho_v)\mu_l g}{x_{sup}^2 (1 - x_{sup})\pi^3}\right]^{\frac{1}{3}} + 20 - 40x_{sup}^2 \quad (16)$$

$$x_{IA} = \left\{\left[0.2914\left(\frac{\rho_v}{\rho_l}\right)^{-\frac{1}{1.75}}\left(\frac{\mu_l}{\mu_v}\right)^{-\frac{1}{7}}\right] + 1\right\}^{-1} \quad (17)$$

2.3 Overview of the model

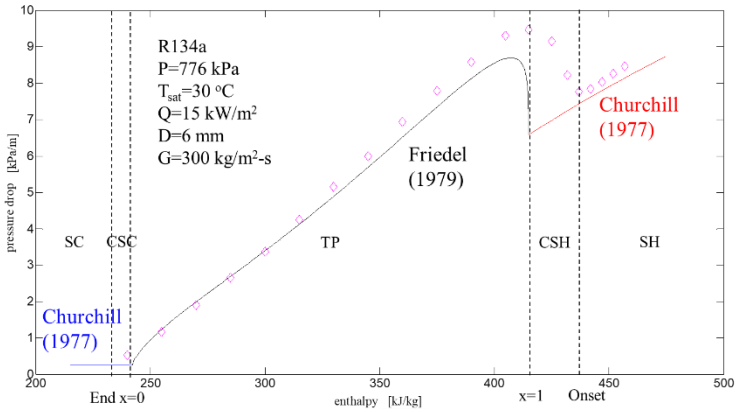

Figure 1: Comparison between pressure drop data and 2 different models ("3-zone" and this model).

Fig.1 is a comparison between experimental data by Xiao and Hrnjak (2018) and two different types of models. The first type, namely the "3-zone" model with Churchill (1977) and Friedel (1979) underpredicts the pressure drop in the CSH region because there is no way a single-phase pressure drop correlation is able to incorporate two-phase mechanisms in it. By tracking the film development under non-equilibrium assumptions, however, the real onset and end of the condensation can be figured out. Parameters like slip velocity, interfacial waviness and flow regime that affect the pressure drop can be calculated knowing the superficial velocity. Therefore, the current model to be presented in this paper fixed the problems in the "3-zone" model and gives more realistic and accurate predictions. The following paragraphs detail the making of the new mechanistic model.

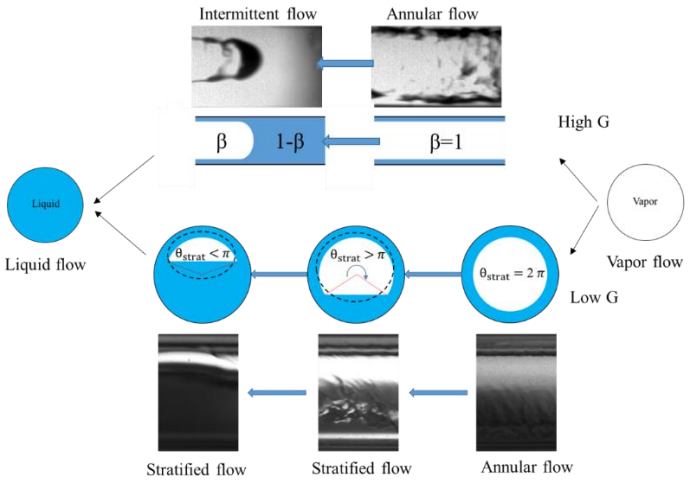

Figure 2: The general structure of the new model.

Fig. 2 presents the two different paths a condensation process can take. As emphasized before, the flow regime at early stages of the condensation has to be annular. When the mass flux is low, the shear force provided by the core vapor cannot move liquid film downstream fast enough. As a result, the gravitational force is able to bring more liquid to the bottom to make the film thickness much thicker at bottom than top. In this case, the flow regime transition happens from annular to the stratified-wavy. When the mass flux is high, the pulling by the interfacial shear is much stronger. The film at the top of the tube is mainly going horizontally than to the bottom. Then the transition of flow regime is from annular to intermittent because eventually the wave have to wash up to the top to block the cross section of the tube when liquid load gets sufficiently large.

2.4 Wave-enhancement factor

$$v_{min} = \left[\frac{2(\rho_l - \rho_v)}{\rho_l}\right]^{0.5} \left[\frac{\sigma(\rho_l - \rho_v)g}{\rho_v^2}\right]^{0.25} \tag{18}$$

$$\delta_{crit} = 2\pi \left[\frac{\sigma \mathrm{g}}{\rho_l - \rho_v}\right]^{0.5} \tag{19}$$

$$\mathrm{K_i} = 1 + C \left(\frac{u_v - u_l}{u_{min}}\right)^{\mathrm{p}} \left(\frac{\delta}{\delta_{crit}}\right)^{q} \tag{20}$$

$$u_v = \frac{G x_{sup}}{\rho_v \varepsilon} \tag{21}$$

$$u_l = \frac{G(1 - x_{sup})}{\rho_l (1 - \varepsilon)} \tag{22}$$

$$\delta = 0.5D(1 - \varepsilon^{0.5}) \tag{23}$$

The wave formation is identified to be one of the two competing factors that creates the peak of pressure drop around bulk quality 1. In literature, the waviness structure also appear in many analysis. Taitel and Dukler (1976) for instance, formulates their transition from stratified flow to intermittent flow with the vapor velocity that generates the growing wave. Generally speaking, the increase of flow velocity triggers the Kelvin-Helmholtz instability. The wave to wash to the top of the tube when there is enough liquid load. Thome et al. (2003) pointed out also that Rayleigh-Taylor instability contribute to the wave generation.

To include Kelvin-Helmholtz instability, the minimum velocity necessary to for the instability to occur is derived in Carey (2008). The equation to find the critical velocity is Eq. (18). Rayleigh-Taylor instability plays a role in this because liquid is placed on top of vapor at the upper part of the tube. The liquid film thickness link the liquid load necessary for a wave to happen to the most dangerous wavelength, which is also introduced by Carey (2008). Eq. (19) is how the wavelength calculated. The wave-enhancement factor $\mathrm{K_i}$ is determined by Eq. (20-22). The film thickness is determined by Eq. (23). Three constants C, p, q are empirically determined to be 2.9, 0.25, and 0.41 respectively.

2.5 Model for single-phase flow

$$J_1 = \left\{-2.457 \ln\left[\left(\frac{7}{Re}\right)^{0.9} + 0.27\left(\frac{e}{d}\right)\right]\right\}^{16} \tag{24}$$

$$J_2 = \left(\frac{37530}{Re}\right)^{16} \tag{25}$$

$$f = 8\left[\left(\frac{8}{Re}\right)^{12} + \left(\frac{1}{J_1 + J_2}\right)^{1.5}\right]^{\frac{1}{12}} \tag{26}$$

$$DP_s = \frac{f G^2}{2\rho D} \tag{27}$$

The single-phase pressure drop is calculated from Churchill (1977) correlation in this paper. Before the onset of condensation and after the end of condensation, Eq. (24-27) are sufficient to find the corresponding pressure drop. In the next subsections, the single-phase correlation used for the two-phase pressure drop calculation is still Churchill

correlation. Other single-phase correlations is potentially capable of replacing the Churchill correlation depending on the application. As long as it is kept consistent in all equations, there should not be a problem of incompatibility.

2.6 Model for annular flow

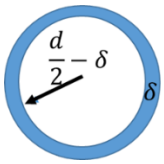

Figure 3: Film structure of the annular flow

$$\dot{E_d} = \dot{E_{dl}} + \dot{E_{dv}} \tag{28}$$

$$\frac{DP}{\rho} = DP_v \frac{x_{sup}}{\rho_v} + DP_l \frac{1 - x_{sup}}{\rho_l} \tag{29}$$

$$\rho = \left(\frac{x_{sup}}{\rho_v} + \frac{1 - x_{sup}}{\rho_l}\right)^{-1} \tag{30}$$

$$DP_v = DP_s K_i \tag{31}$$

$$DP_l = DP_s \left(\frac{D}{2\delta}\right)^m K_i \tag{32}$$

The annular flow is assumed to be a ring of liquid film wrapping around the core vapor. The film thickness is assumed to be uniform. The pressure drop is considered as the measure of energy dissipation. The dissipation in vapor flow can be treated as if the liquid-vapor interface is the rough surface that drags the vapor flow. The dissipation in liquid flow is more complicated in that it is flowing in between two surfaces: the interface and the tube wall. Wave-enhancement factor is incorporated into the equations to account for the effects from the waves. Eq. (28-32) together with Eq. (18-27) calculate the total pressure drop of an annular flow.

2.7 Model for stratified flow

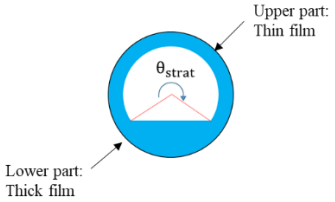

Figure 4: Film structure of the stratified flow

$$DP = DP_{upper} \frac{\theta_{strat}}{2\pi} + DP_{lower} \frac{2\pi - \theta_{strat}}{2\pi} \tag{33}$$

$$DP_{upper} = DP_{v,upper} \frac{\rho}{\rho_v} x_{sup} + DP_{l,upper} \frac{\rho}{\rho_l}(1 - x_{sup}) \tag{34}$$

$$DP_{v,upper} = DP_{s,upper} K_{i,upper} \tag{35}$$

$$DP_{l,upper} = DP_{s,upper} \left(\frac{D}{2\delta_{trans}}\right)^m K_{i,upper} \tag{36}$$

$$DP_{lower} = DP_v \frac{\rho}{\rho_v} x_{sup} + DP_l \frac{\rho}{\rho_l}(1 - x_{sup}) \tag{37}$$

$$\delta_{lower} = 0.5d[1 - \frac{\sin(2\pi - \theta_{strat})}{2\pi - \theta_{stat}}] \tag{38}$$

$$DP_{v,lower} = DP_{s,lower} K_{i,lower} \tag{39}$$

$$DP_{l,lower} = DP_{s,upper}\left(\frac{D}{2\delta_{eq}}\right)^{m} K_{i,lower} \tag{40}$$

$$\rho = \left(\frac{x_{sup}}{\rho_v} + \frac{1 - x_{sup}}{\rho_l}\right)^{-1} \tag{41}$$

$$1 - \varepsilon = \frac{1}{2}[(2\pi - \theta_{strat}) - \sin(2\pi - \theta_{strat}) + \theta_{strat}(1 - \varepsilon_{trans})] \tag{42}$$

The stratified flow is essentially annular flow with extra condensate that cannot be held at the top. Therefore, the upper part and the lower part of the tube should be separately treated. Usually the liquid pool at the lower part of the tube is treated like single-phase liquid. Started from Chato and Dobson (1998), furthered by Thome et al. (2003), Macdonald and Garimella (2016) and Xiao and Hrnjak (2017), the flow at the upper part of the tube is considered essentially a continuation of annular flow with new condensate going downward and forward, while the flow at the lower part of the tube is handled as an annular flow moving towards single-phase liquid flow. The film thickness is the key parameter that linked the transition from annular to stratified and eventually single-phase flow. The stratification angle is calculated through iteration from Eq. (42). When the stratification angle reaches 180 degrees and above, the film thickness of the lower part of the tube is set to half of the diameter. The total pressure drop of a stratified flow can be calculated form Eq. (18-42).

2.8 Model for intermittent flow

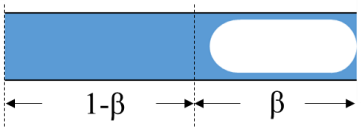

Figure 5: Film structure of the intermittent flow

$$DP = \beta DP_{annular} + (1 - \beta)DP_{liquid} \tag{43}$$

$$DP_{annular} = DP_{v,annular}\frac{\rho}{\rho_v}\, x_{sup} + DP_{l,annular}\frac{\rho}{\rho_l}(1 - x_{sup}) \tag{44}$$

$$DP_{v,annular} = DP_{s,annular}K_{i,annular} \tag{45}$$

$$DP_{l,annular} = DP_{s,annular}\left(\frac{D}{2\delta_{trans}}\right)^{m} K_{i,annular} \tag{46}$$

$$DP_{liquid} = DP_{s,liquid} \tag{47}$$

$$\rho = \left(\frac{x_{sup}}{\rho_v} + \frac{1 - x_{sup}}{\rho_l}\right)^{-1} \tag{48}$$

$$\beta = \frac{\varepsilon}{\varepsilon_{trans}} \tag{49}$$

The intermittent flow is different from the stratified flow in that it does not separate the tube into the upper and lower part. Due to the periodical nature of the waves, the complete blockage of the tube cross section happens only at some segments of the tube. Therefore, the liquid slug and the elongated bubble should be treated differently. For liquid slug, though not the same as a single-phase liquid flow, its pressure drop should be very close to the single-phase scenario. The effects on pressure drop from waves, pulls from vapor etc. are all non-existent in a liquid slug after all. For the elongated bubble, except the two ends, it is basically an annular flow. Thus the pressure drop at the annular-intermittent flow regime transition is used for elongated bubbles throughout the intermittent flow.

3. MODEL VALIDATION

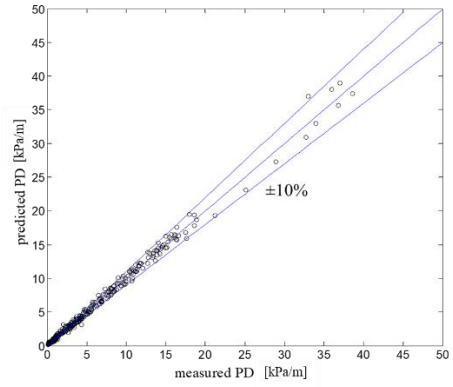

Figure 6: Comparison between the predictions from the current model and the experimental data.

Fig. 6 is an overall comparison between the predictions from the current model and the experimental data from Xiao and Hrnjak (2018) including R32, R134a, R1234ze(E), R1233zd(E) and R245fa in tube size of 6.1 and 4.0 mm at heat fluxes of 5 to15 kW/m^2 and mass flux of 100 to 400 kg/m^2-s. As far as the authors realize, these data are from the only study that includes the non-equilibrium effects on the pressure drop in a condenser of a vapor-compression system. Most predictions of the new model fall into the ±10% deviations of the experimental data, indicating statistically good predictability.

4. CONCLUSIONS

A new pressure drop model is proposed for the condensation process from superheated vapor. It is especially applicable to a condenser with horizontal smooth round tube in a vapor-compression system where non-equilibrium always exist. The model traces the heat transfer process to find the real onset and end of condensation. With the void fraction and flow regime map developed under diabatic conditions, the path a two-phase flow can take is divided into two different conditions. One is from annular to intermittent flow when the mass flux is high. The other is from annular to stratified flow when the mass flux is low. Equations for each flow regime are developed. With the current approach, the most important mechanisms that the authors deem important are explained and included. In this way the model attempts to be both accurate and general, and hopefully be able to provide useful insight for the future studies. The model is validated by experimental data for a wide range of refrigerants under different working conditions in two different diameter tubes.

NOMENCLATURE

SH	Superheated
CSH	Condensing superheated
TP	Two-phase
CSC	Condensing subcooled
SC	Subcooled
Re	Reynolds number
We	Webber number
Fr	Froude number
x	Thermal dynamic quality
ε	Void fraction
K	Wave-enhancement number

PD	Pressure drop	(Pa/m)
A	Area	(m^2)
HTC	Heat transfer coefficient	(W/m^2-K)
T	Temperature	(K)
P	Pressure	(Pa)
G	Mass flux	($kg/s-m^2$)
Q	Heat flux	(kW/m^2)
D	Tube diameter	(mm)
ρ	Density	(kg/m^3)
μ	Dynamic viscosity	(kg/m-s)
σ	Surface tension	(N/m)
h	Specific enthalpy	(J/kg)
E	Energy	(J)
e	Surface roughness	(m)
δ	Thickness	(m)
u	velocity	(m/s)
g	Acceleration of gravity	(m/s^2)

Subscripts

b	Bulk
sat	Saturated
sup	Superficial
l	Liquid
v	Vapor
s	Single phase
d	Dissipated
trans	Transition
crit	Critical
min	Minimum
crit	Critical
upper	Upper part of the tube
lower	Lower part of the tube
onset	Onset of condensation
end	End of condensation

REFERENCES

Agarwal, R., Hrnjak, P., 2015, Condensation in two phase and desuperheating zone for R1234ze(E), R134a and R32 in horizontal smooth tubes, *Int. J. Refrigeration*, vol. 50, p. 172-183.

Carey, V.P., 2008, Liquid–Vapor Phase-Change Phenomena, *CRC Press*.

Churchill, S.W., 1977, Friction-factor equation spans all fluid-flow regimes. *Chem. Eng*, vol. 7, p. 91–92.

Dittus, F., Boelter, L., 1930, *University of California Publications on Engineering*, 0096-9311.

Dobson, M.K., Chato, J.C., 1998, Condensation in smooth horizontal tubes, *J. Heat Transfer*, vol. 120, p. 193–213.

El Hajal, J., Thome, J.R., Cavallini, A., 2003, Condensation in horizontal tubes, Part 1: Two-phase flow pattern map, *Int. J. Heat Mass Transfer*, vol. 46, no. 18, p. 3349–3363.

Gnielinski, V., 1976, New equation of heat and mass transfer in turbulent pipe and channel flow, *Int. Chem. Eng.*, vol. 16, p. 359-367.

Kondou, C., Hrnjak, P., 2011a, Heat rejection from R744 flow under uniform temperature cooling in a horizontal smooth tube around the critical point, *Int. J. Refrigeration*, vol. 34, no. 3, p. 719-731.

Kondou, C., Hrnjak, P., 2011b, Heat rejection in condensers close to critical point-desuperheating, condensation in superheated region and condensation of two phase fluid, *Int. Conf. Heat Trans. Fluid Mech. and Thermodynamics*, Mauritius.

Kondou, C., Hrnjak, P., 2012, Condensation from superheated vapor flow of R744 and R410A at subcritical pressures in a horizontal smooth tube, *Int. J. Heat Mass Transfer,* vol. 55, p. 2779-2791.

Macdonald, M., Garimella, S., 2016, Hydrocarbon condensation in horizontal smooth tubes: Part II – Heat transfer coefficient and pressure drop modeling, *Int. J. Heat Mass Transfer,* vol. 93, p. 1248–1261.

Meyer, M., Hrnjak, P., 2017, Flow regimes during condensation in superheated zone, *Int. J. Refrigerant,* vol. 84, p. 336-343.

Rouhani, Z., Axelsson, E., 1970, Calculation of void volume fraction in the subcooled and quality boiling regions, *Int. J. Heat Mass Transfer,* vol. 13, p. 383–393.

Taitel, Y., Dukler, A.E., 1976, A model for predicting flow regime transitions in horizontal and near horizontal gas–liquid flow, *AIChE J.*, vol. 22, no. 1, p. 47–54.

Xiao, J., Hrnjak, P., 2016, Heat transfer and pressure drop of condensation from superheated vapor to subcooled liquid, *Int. J. Heat Mass Transfer,* vol. 103, p. 1327-1334.

Xiao, J., Hrnjak, P., 2017a, A new flow regime map and void fraction model based on the flow characterization of condensation, *Int. J. Heat Mass Transfer,* vol. 108, p. 443-452.

Xiao, J., Hrnjak, P., 2017b, A heat transfer model for condensation accounting for non-equilibrium effects, *Int. J. Heat Mass Transfer,* vol. 111, p. 201-210.

Xiao, J., Hrnjak, P., 2018, Pressure drop of R134a, R32 and R1233zd(E) in diabatic conditions during condensation from superheated vapor, *Int. J. Heat Mass Transfer,* vol. 122, p. 442-450.

ACKNOWLEDGEMENT

The authors thankfully acknowledge the support provided by the Air Conditioning and Refrigeration Center at the University of Illinois at Urbana-Champaign and technical support from Creative Thermal Solutions, Inc. (CTS).